CHAPTER 3

SYNTHESIS AND CHARACTERIZATION OF NANOPARTICLE AND NANOCOMPOSITE MEMBRANE

Nano-particles of Titanium dioxide (TiO_2) have been prepared through the green route using extract of *Cajanus cajan* seeds as the capping and stabilizing medium. The synthesized particles have been characterized and incorporated into polyvinylidene fluoride (PVDF) membranes to get hydrophilic composite membranes. Spectroscopic and microscopic techniques have been used to characterize the composite membranes. The X-ray diffraction analysis confirmed the anatase phase of titanium dioxide nanoparticles of crystallite size 15.89 nm. The effect of titanium dioxide concentration on the thermodynamic and rheological properties on the polyvinylidene fluoride casting solution has been investigated using the triangular phase diagram and solution viscosity measurements. Mathematical modeling of a phase inversion membrane was studied to predict the morphology. It has been observed that addition of green synthesized TiO_2 increases the viscosity, and after addition of a sufficient amount results in the formation of two phases. Thermodynamics enhances the de-mixing rate, whereas kinetics delays the mixing rate; the trade-off between the two affects the membrane morphology, hence kinetic and thermodynamic parameters have been evaluated and analyzed. The phase diagrams for PVDF/ TiO_2/solvent/Water system have been drawn experimentally at different concentrations of TiO_2 using a new method. Synthesized membranes have been characterized by measuring contact angle, porosity, and permeability. The surface morphology at different compositions has also been examined using High-Resolution Scanning Electron Microscope (HRSEM) technique.

3.1 INTRODUCTION

Application of membranes for the treatment of water and wastewater in food and dairy industries is increasing rapidly (Jung et al., 2016). Efficacy of the membrane depends on its porosity, morphology, hydrophilicity, and surface roughness (Kurada et al., 2017). Incorporating additives into the membrane casting solution is an efficient method to enhance the performance of the resultant membrane through the alteration in its permeation property and separation efficiency (Sadrzadeh and Bhattacharjee 2013). The membrane morphology strongly affects the permeation and separation parameters. The thermodynamic and kinetics interactions determine the morphology of the membrane during membrane fabrication. Thus it is essential to understand the importance of thermodynamic and kinetic parameters. The thermodynamic parameters define the porosity and morphology, and the kinetic parameters control the surface hydrophilicity and roughness and, thus, the antifouling property of the membrane (Kurada et al., 2017).

Thermodynamic and kinetic properties of the polymeric casting solution affect the demixing phenomenon and precipitation rate (Shieh and Chung 1998). The authors concluded that a dense membrane forms due to delayed liquid-liquid demixing compared to instant liquid-liquid demixing. Mohsenpour et al. (2016) in their study highlighted the effect of liquid-liquid demixing on the morphology of the membrane. The binodal line in the phase diagram is used extensively to study the thermodynamic instability. The effect of polymer molecular weight (MW) on the morphology and performance of the membranes by tuning the thermodynamic and kinetic hindrances of the membranes were also reported (Sadrzadeh and Bhattacharjee 2013). Experimental and theoretical studies of thermodynamics have been extensively carried out for a large number of polymers such as

cellulose acetate (Reuvers et al., 1986), polyethersulfone (Wei et al., 2006), polyacrylonitrile (Tan et al., 2008), etc. Polyvinylidene fluoride (PVDF) is the widely used polymer for the fabrication of membranes due to the high thermal stability attributed to high carbon-fluorine dissociation energy and chemical resistance to corrosive materials like halogens, oxidants, and inorganic acids, etc. (Yeow et al., 2009) and comparatively cheaper than other mentioned polymers also no specific category of solvent is required to dissolve this polymer like in case of polysulfones, cellulose acetate which require protic solvent and add cost to synthesis and their stability is also very poor. The PVDF membranes are used in ultrafiltration, nanofiltration, membrane bio-reactor for wastewater treatment, but their high hydrophobicity of PVDF results in extreme fouling hence limits its application. The drawback of using pristine PVDF was overcome by enhancing the polymer property using nanoparticle as an additive. Out of different nanoparticles existing, titanium dioxide (TiO_2) is widely used because of its low energy band gap, eco-friendliness, easy of processing and cost-effectiveness. Industrially TiO_2 is made using Sulfate process or the Chloride process and the main raw materials include ilmenite (FeO/TiO_2), or titanium slag. Sulfate process generally has higher production costs and with acid treatment is more expensive and chloride require chloralkali unit and difficult to operate because of the high temperature chlorine (900 – 1000°C) requirement

In view of this an attempt has been made to synthesize TiO_2 nanoparticles because from many literatures (Moro et al., 2015, Jain and Vaya 2017, Si et al., 2019) it was concluded that not much significant difference in the catalytic activity was observed when compared with commercially available particle. So from economic point of view TiO_2 nanoparticles was synthesized from the extract of *Cajanus Cajan* seeds (obtained easily

from kitchen waste thus avoiding the use of a costly chemical reducing agent and/or capping or stabilizing agent). The presence of active substance Terpenoids, Aliphatic, and Aromatic amines (active substance) in extract result in efficient stabilization and avoid agglomeration of NPs (Arif et al., 2019). Also here effect of loading of synthesized TiO_2 as an additive to the PVDF membrane morphology is discussed in terms of thermodynamic and kinetic parameters and the role of thermo-kinetic property on the permeability is investigated. Mathematical modeling of a phase inversion membrane using green synthesized TiO_2 NPs embedded in polymer matrix is carried out for the first time. A systematic investigation of the particle interaction with the polymer solution during phase inversion in membrane fabrication is carried to understand the effect of additive incorporation in changing the membrane morphology in terms of a thermodynamic and kinetic parameter, which is rarely known. The phase behaviour is studied experimentally for PVDF/TiO_2/NMP/Water system. The thermodynamic and kinetic parameters are evaluated at different loadings of TiO_2 to obtain a relation between membrane structure and these two parameters. The synthesized membranes are also characterized by measuring the viscosity of casting solution, and membrane morphology, contact angle, pore size, porosity, and permeability. Membrane performance is analyzed in terms of hexavalent chromium (Cr(VI) removal to understand the importance of thermodynamic and kinetic parameters on the membrane morphology.

3.1.2 Theory of Membrane Formation:

3.1.2.a Phase Diagram and Thermodynamic Parameter

The ternary and quaternary phase diagrams are used to evaluate the thermodynamic parameter. In the phase diagram initially, the binary polymeric solution is on

polymer/solvent line. Introduction of a non-solvent into a polymeric/solvent solution results in the precipitation of the solution. This difference in the polymer/solvent and the binodal line is called the miscibility gap (MG). Incorporation of additives alters the binodal path; as a result, MG also changes. The degree of shift in the binodal curve (DSBC) is evaluated using equation (3.1) (Mohsenpour and Khosravanian 2018).

$$DSBC = (MG_{additive} - MG_{without\ additive}) / MG_{additive} \quad (3.1)$$

A non-dimensional thermodynamic parameter TE, defined by equation (3.2) is used to evaluate the effect of thermodynamic enhancement

$$TE = DSBC \times g_{solvent/additive} \quad (3.2)$$

where $g_{solvent/additive}$ is the interaction parameter and can be calculated using equation (3.3)

$$g_{solvent/additive} = 0.6v_1/RT\ [(\delta_{1,d} - \delta_{2,d})^2 + 0.25(\delta_{1,p} - \delta_{2,p})^2 + 0.25(\delta_{1,h} - \delta_{2,h})^2] \quad (3.3)$$

where, δ is the Hasen solubility parameter, δ_d, δ_p, δ_h represent the dispersive interaction, polar interaction, hydrogen bond ($MPa^{0.5}$) respectively, and subscripts 1 & 2 represent solvent and additive (non-solvent), respectively. The values of Hanson's solubility parameters of components, were adopted from the literature and are given in Table 3.1 (Dai et al., 2010, Oh et al., 2009).

Table 3.1: Hanson solubility parameters of membrane components

Component	**$\delta_{i,p}$**	**$\delta_{i,h}$**	**$\delta_{i,d}$**
PVDF	12.5	17.2	9.2
TiO_2	15.16	15.14	5.18
NMP	12.3	18	7.2
Water	16	42.3	15.6

3.1.2.b Kinetic parameter

When a polymeric casting solution is placed in a non-solvent bath, precipitation takes place because of the exchange of solvent and non-solvent (mass transfer). Precipitation rate determines the membrane morphology. Patsis and Henriques (Mohsenpour and Khosravanian, 2018) evaluated the effect of solvent concentration in a non-solvent bath as a function of time using two differential equations that include the skin layer growth $\frac{dy}{dt}$ (equation 3.4) and volume change of the diffusing solvent $\frac{ds}{dt}$ (equation 3.5)

$$\frac{dy}{dt} = \Upsilon D_{ns} \frac{\widehat{C_{ns}}}{y(t)} \quad (3.4)$$

$$\frac{ds}{dt} = a \frac{C_o D_s}{y(t)} \quad (3.5)$$

where $\frac{dy_t}{dt}$ indicates the growth rate, subscripts s, and ns represent solvent and non-solvent, respectively. D is the diffusion coefficient, C is the volume fraction, s is the solvent volume,

$\widehat{C_{ns}}$ is the volume fraction of pure non-solvent ($\widehat{C_{ns}}$ = 1), C_o is the volume fraction of the solvent on the film surface next to polymer solution (C_o=1), 'a' is the film area (0.05 m^2), and Υ is the compacting factor (Υ=1) (as polymer density is almost equal to the density of synthesized membrane). Combining and solving equations (3.4) and (3.5) gives solvent volume in non-solvent as shown in equation (3.6)

$$\frac{C_t}{C_\infty} = \frac{\sqrt{2} a D_{sa} C_m}{V\sqrt{\Upsilon D_{ns} \widehat{C_{ns}}}} (t^{0.5} - t_0^{0.5}) \quad (3.6)$$

where C_∞ is the final solvent concentration in the non-solvent is measured by the total organic carbon analyser**,** D_{sa} is the diffusion coefficient of solvent and additive, t_0 refers to

time lag for sensing organics, V is the non-solvent volume (1 L), and $C_m=\frac{C_o}{C_\infty}$. Plot of $\frac{C_t}{C_\infty}$ (solvent concentration) vs. $t^{0.5}$ produces a straight line with slope (m)

$$m = \frac{\sqrt{2}aD_{sa}\,C_m}{V\sqrt{\Upsilon D_{ns}C_{ns}}} = \frac{0.071D_{sa}}{C_\infty\sqrt{D_{ns}}} = \beta\frac{D_{sa}}{\sqrt{D_{ns}}} \quad (3.7)$$

'm' value from the graph between $\frac{C_t}{C_\infty}$ vs $t^{0.5}$ is used to evaluate $\frac{D_{sa}}{\sqrt{D_{ns}}}$ value using equation (3.7). The kinetic parameter (k), a dimensionless parameter is now defined by equation (3.8)

$$k= \frac{M_p D_{sa}}{a\mu_p t^{0.5}\sqrt{D_{ns}}} \quad (3.8)$$

where M_p and μ_p represent mass and viscosity of the polymeric solution. Their values will change with additive concentration.

A series of membrane casting solutions were prepared by varying the amounts of polymer, solvent, non-solvent and additives and their phase behaviour, viscosity were investigated to know the thermodynamic and kinetic parameters before casting the membranes. The prepared membranes were then evaluated for their performance and antifouling characteristics. The details of these experiments and their results are described in following sections.

3.2 EXPERIMENTAL PROCEDURE

3.2.1 Materials

Polyvinylidene fluoride (PVDF) polymer (M_W= 534,000), n-methyl-2-pyrrolidone solvent (NMP), and Titanium Isopropoxide (TTIP) were purchased from Sigma-Aldrich

(Bombay, India). *Cajanus Cajan* seeds were collected from IIT(BHU) campus. The double distilled water (DD) prepared in the laboratory was used as the non-solvent.

3.2.2 Method

3.2.2.a Synthesis of TiO_2 Nanoparticles (NPs)

Splitted seeds of *Cajanus cajan* (Arhar pulse (Dal)) were washed thoroughly using tap water to remove surface dust. 15 g of the washed seeds in 75 mL DD water were taken in a beaker and heated at 60 °C for 5 h. The extract (yellow color) was collected using a Whatman No-01 filter paper and stored for future use. Solution of TTIP (165 mL, 5mM TTIP) was prepared in beaker by dissolving 1.42 g of TTIP in 165 mL water to which 45 ml of extract was added. The mixture was stirred continuously for 7-8h at ambient temperature. The precipitate obtained at the bottom of the beaker was centrifuged using a High-Speed Research Centrifuge (TC 4100 F, Eltek, Bombay, India) at 6,000 rpm for 1 h to separate the yellow powder from the extract. The yellow colored powder was dried at 80 °C for 4 h air oven followed by calcination at 550 °C in a muffle furnace for 3 h to obtain a white color powder. The powder obtained was collected and stored in vial and is characterized with different technique to ensure that TiO_2 nanoparticle is formed. This synthesized particle is then incorporated in polymer during membrane synthesis in different amount to obtain nanocomposite membrane.

3.2.2.b PVDF/TiO_2 composite membranes preparation

The PVDF composite membranes were fabricated using the phase-inversion technique. Initially, the PVDF polymer and TiO_2 were dried in an oven at 85°C for 2 h. In the meantime, the known amount of PVDF polymer (8 g dry pellets) was dissolved in 40 ml

the organic solvent n-methyl-2-pyrrolidone (NMP) and was placed on a hot plate with magnetic stirrer and heated to 65-70°C to get a homogeneous solution. Simultaneously different amounts of TiO_2 powder were dispersed in 4 ml of NMP by sonication for 1 h. The suspensions of TiO_2/NMP thus prepared were added gradually to the PVDF/NMP solution prepared earlier. The solutions were mixed by agitating for 8 h at 65-70°C to obtain a uniform suspension. The viscosity of the solution was measured using a digital rotational viscometer (LMDV-60, Labman, Bombay, India) at ambient temperature. The solution was then cast into a thin film with a clearance of 180 µm on a glass plate. The cast film was exposed to air for 60 s and then put in a water bath (non-solvent) at the ambient temperature (27±1 °C) for 8 h for complete exchange of solvent and non-solvent. The fabricated membranes were peeled off from the glass plates, washed, and stored in DI water for further study. Membranes of different wt% of PVDF/TiO_2 is marked as PM1 (0wt% TiO_2), PM2 (1wt% TiO_2), PM3 (2wt% TiO_2) and PM4 (3wt% TiO_2). Schematic representations of nano-particle and polymer film synthesis are shown in Figure 3.1

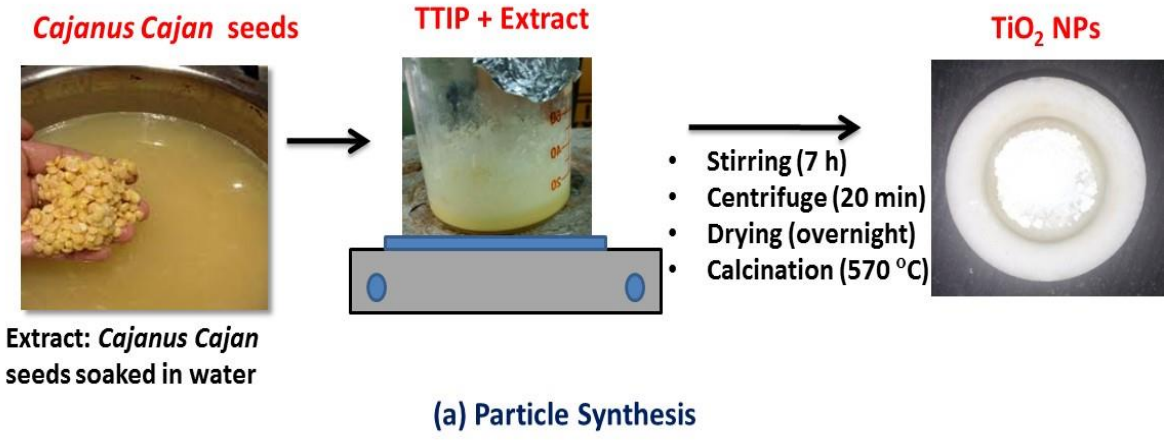

Figure 3.1: (a) Schematic representation for synthesis of TiO_2 particle and

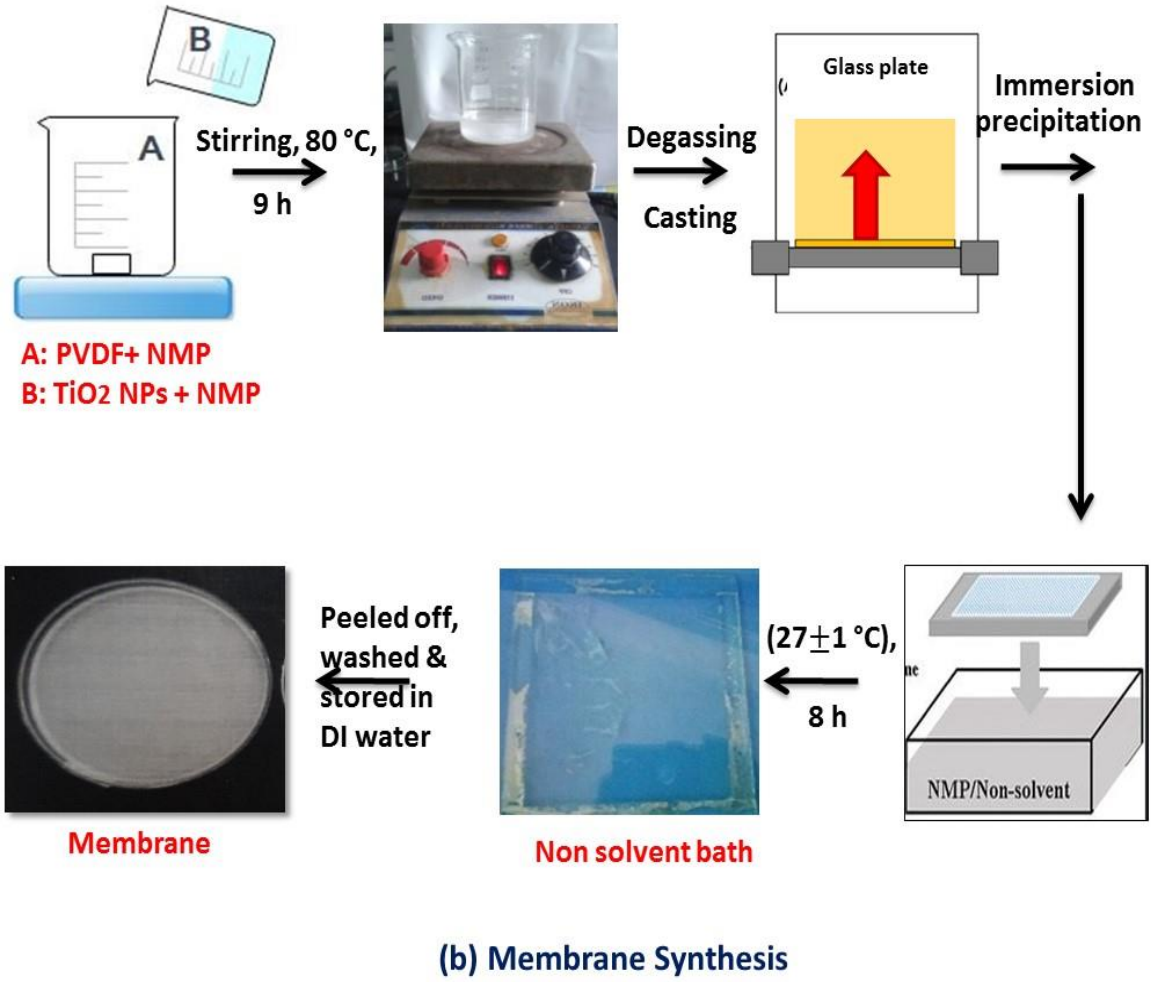

Figure 3.1: (b) Schematic representation for membrane synthesis

3.2.3 Determination of Thermodynamic Parameter

The turbidimetric titration method was used to evaluate the cloud points of polymeric solutions at 25 °C. A homogeneous solution of PVDF/NMP of known concentration was prepared. Simultaneously TiO_2 powder was added to 4 mL of NMP taken in a beaker, sonicated for 30 min and then added slowly to the polymeric solution. The PVDF/TiO_2/NMP solution was continuously agitated and titrated with non-solvent (i.e., deionized water). The non-solvent was added drop wise using a 0.1-mL syringe until the solution just became turbid which was clearly recognized by direct visualization.

For viscous polymeric solutions, titration was carried out at the elevated temperature of 60–70 °C and then cooled to 25 °C; if turbidity was not observed at 25 °C, more water was again added drop wise. The amount of water used to attain the cloud point was recorded. The ternary phase diagram was prepared with the help of cloud point values by calculating the weight fractions of PVDF (polymer), NMP (solvent), and water (non-solvent).

3.2.4 Determination of Kinetic Parameter

The PVDF/TiO_2 composite membranes were prepared from the polymer solution with different loadings of TiO_2 by casting onto a glass plate and then immersing into a deionized water bath at ambient temperature. The kinetic measurement was carried out by calculating the exchange rate between the solvent and the non-solvent. The instantaneous concentration of solvent in the water bath was measured by taking out samples near the film surface using a microsyringe and analyzing it using a Shimadzu total organic carbon analyzer (TOC-500, Shimadzu, Kyoto, Japan).

3.2.5 Membrane characteristics

The wetting ability of membranes was evaluated by measuring the contact angle between the probe liquid and the membrane surface at ambient temperature using a contact angle goniometer [KRUSS, DSA 4, Germany] using the sessile drop method. Each test was conducted in triplicates to ensure accuracy and average values were used.

The membrane porosity (ε) and pore size (r_m) were calculated using simple equations (3.9) & (3.10) (Mohsenpour and Khosravanian, 2018). The membrane sheet of area (a =1 × 1 cm^2), thickness (l) was initially weighed as W_1 and then dipped in distilled

water at room temperature for 24 h. Then, the sample pieces were removed and blotted with filter paper and weighed immediately as W_2.

$$\varepsilon = W_1 - W_2 / (a \times l \times \rho_w) \quad (3.9)$$

$$r_m = \sqrt{\frac{(2.9-1.7\varepsilon) \times 8\mu_w \times l \times J}{\varepsilon \times a \times \Delta P}} \quad (3.10a)$$

where ρ_w is the density of water

Tortuosity (τ) shows an inverse relationship with porosity and could be calculated using Eq. (3.10b)

$$\tau = (2 - \varepsilon)^2 / \varepsilon \quad (3.10b)$$

3.2.6 Characterization Techniques

The nano-particles of TiO_2 synthesized through green route were characterized in terms of particle shape and size and the membranes were characterized by measuring the contact angle and FTIR spectroscopy. The basic details of various instruments used for this purpose are given below.

High Resolution Transmission Electron Microscope (HRTEM): Particle shape and size was analysed using a High Resolution Transmission Electron Microscope (HR- TEM, Model: Tecnai G2 20 TWIN of USA (S.E.A.) PTE, LTD**,** USA)

X-Ray Diffractometer (XRD): Smart Lab X-Ray Diffractometer (Rigaku Smart Lab Powder type, without χ-cradle, Japan) was used to confirm the synthesis of TiO_2 NPs. It is operated at 18KW and consists of a rotating anode XRD (1200–1800 K temperature, CuKα radiation of λ 1.5406 Å).

Particle Size Analyzer: Nano Plus (Zeta/nanosize analyzer, Micromeritics Instrument Corp. India) working on the principle of dynamic light scattering (DLS) technique was used to define the average particle size.

Contact Angle Analyzer: Wetting property of membrane was analyzed using contact angle goniometer [KRUSS, DSA 4, Germany] by sessile drop method using two μL DI water as probe liquid.

Fourier Transform Infrared (FTIR) Spectroscopy: The FTIR spectra of nano-composite membranes were recorded on TIR (02) [Perkin Elmer, Bruker, US] in the range of 500–4000 cm^{-1}.

Diffusive Reflectance Spectroscopy (DRS): Studies for the Optical band gap were carried out using CARY-100 Bio UV–Visible spectrophotometer, wavelength ranging from 200 to 1000 nm.

3.3 RESULTS AND DISCUSSION

3.3.1 Particle and Membrane Characterization

3.3.1.a High Resolution Transmission Electron Microscope (HRTEM) Results

The HRTEM image (Figure 3.2a) reveals spherical shape of particle in the size ranges of 07 to 09 nm with an average size of around 8.5 nm. Polycrystalline anatase structure was confirmed from the Selected Area Diffraction (SAD) pattern as shown in Figure 3.2b. Similar results are also reported in the literature (Dai et al., 2010).

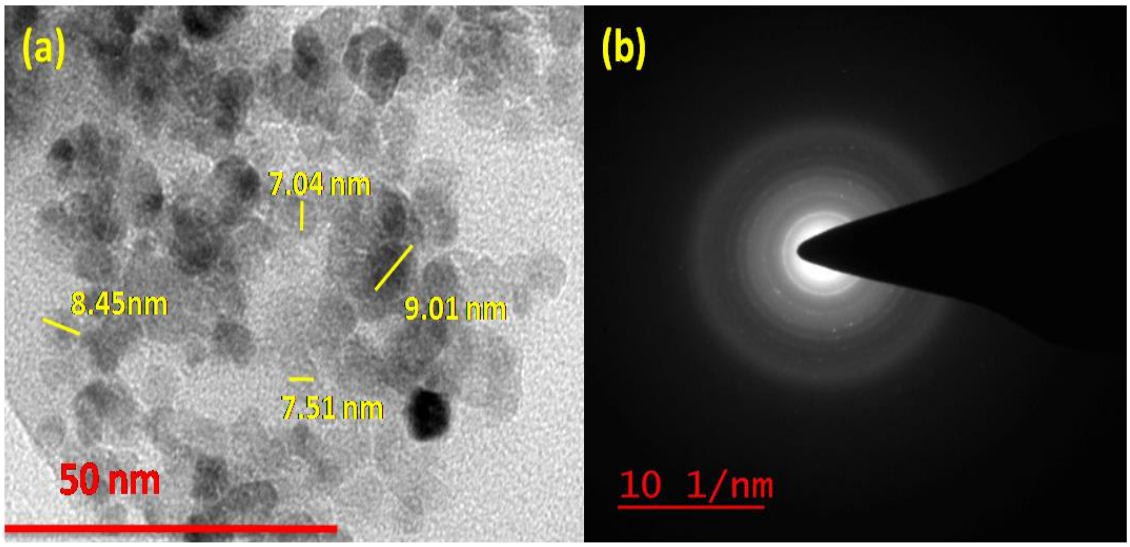

Figure 3.2: (a) HRTEM image of TiO_2 NPs, (b) SAED pattern of TiO_2 NPs

3.3.1.b X-Ray Diffractometer (XRD) Finger Prints

The formation of TiO_2 NPs was confirmed from the XRD patterns, as shown in Figure 3.3a. The sharp diffraction peak intensity indicates the excellent crystalline structure. The diffraction peaks obtained at 2θ of 25.4°, 37.9°, 48.02°, 54.02°, 55.3°, 68.97° and 75.9 signifies the anatase phase of TiO_2 NPs and corresponding Miller indices (hkl) values are (101),(004),(200),(105),(211),(116),(215). The obtained peaks match with peaks mentioned in the JCPDS 21-1272 Handbook, confirming the successful formation of TiO_2 NPs (Li et al. 2014). The Debye Scherrer's equation was used to calculate the crystalline size of the particle as

$$d = 0.89 \lambda / \beta \cos \theta \qquad (3.11)$$

where d represents the crystallite size (nm), λ is the X-ray wavelength (0.154 nm), θ represents the Bragg's diffraction angle, and β is the FWHM (full width at half maximum). The calculated crystallite size of the NPs was found to be 15.89 nm.

The average particle size distribution curve obtained from dynamic light scattering (DLS) technique is shown in Figure 3.3b. The figure depicts the mono-dispersed distribution of particles with an average particle diameter ranging from 20 to 40 nm.

The XRD pattern of membrane depict strong peak at 20.4° implies β-phase of PVDF along with existence of 4 additional peak in case of PVDF/TiO_2 which ensures that particles are well embedded within the polymer matrix as similar peaks were observed in case of pure TiO_2 NPs. However, due to the presence of TiO_2 the peak intensity at 2θ =20.4° is smaller for PVDF/TiO_2 compared to pure PVDF membrane indicating shift towards an amorphous region , hence good for membrane application (Arif et al., 2019).

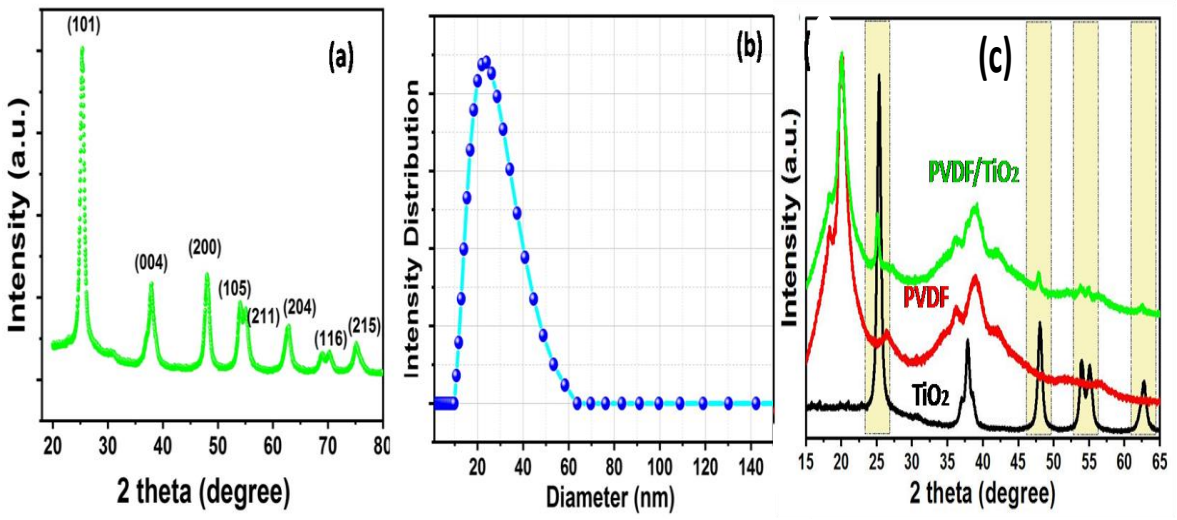

Figure 3.3: (a) XRD pattern, (b) DLS spectra of synthesized TiO_2 NPs, and (c) XRD pattern of TiO_2 NPs, PVDF and PVDF/ TiO_2 membrane

3.3.2.c Fourier Transform Infrared (FTIR) Spectra

The peaks corresponding to different groups in FTIR spectra are shown in Figure 3.4a. The peak at wave number 3748 cm^{-1} is due to -OH groups of water and TiO_2 in the polymer matrix, and peak at wave number 640 cm^{-1} confirm the presence of NPs in PVDF/TiO_2 membrane (Wei et al. 2011). The other peaks in all membranes at wave

number 3748, 1658, 1398, 1171 cm^{-1} corresponds to the functional groups –OH, H-O-H, C-H deformation, C-F stretching respectively whereas the peaks at 640 cm^{-1} in PM2, PM3, PM4 corresponds to Ti-O-Ti group thus confirming the presence of TiO_2 nano-particle within the polymer matrix.

The β-Phase (F(β)) and α-Phase (F(α)) content (%)in the PVDF/TiO_2membrane were calculated using the Lambert-Beer law is given in Equation (3.12)

$$F(\beta)=\frac{a_\beta}{\frac{k_\beta}{k_\alpha}a_\alpha+a_\beta}\times 100 \text{ and } F(\alpha)=\frac{a_\alpha}{\frac{k_\alpha}{k_\beta}a_\beta+a_\alpha}\times 100 \quad (3.12)$$

where a_α and a_β refers to the absorbance value at wave numbers 760 and 860 cm^{-1}, respectively, corresponding to α and β-phases (Vinoth et al. 2019). It was observed that the peak intensity corresponding to the α-phase of PVDF diminished due to the addition of TiO_2 NPs. The β-phase content was calculated using Equation (3.12). The calculated content of β-phase for pure PVDF and PVDF/TiO_2 is shown in Figure 3.4b.The figure depicts that with increasing concentration of TiO_2 there is a shift from the crystalline α-phase to β-phase and maximum shift is achieved for PM3 membrane due to the incorporation of TiO_2 NPs and also due to the interaction between the polymer and the inorganic filler (Vinoth et al.2019) which is desirable because it has been reported in the literature that β-phase is considered as the stable form which results in the enhancement of toughness in nano-composite materials (Lai et al., 2014).

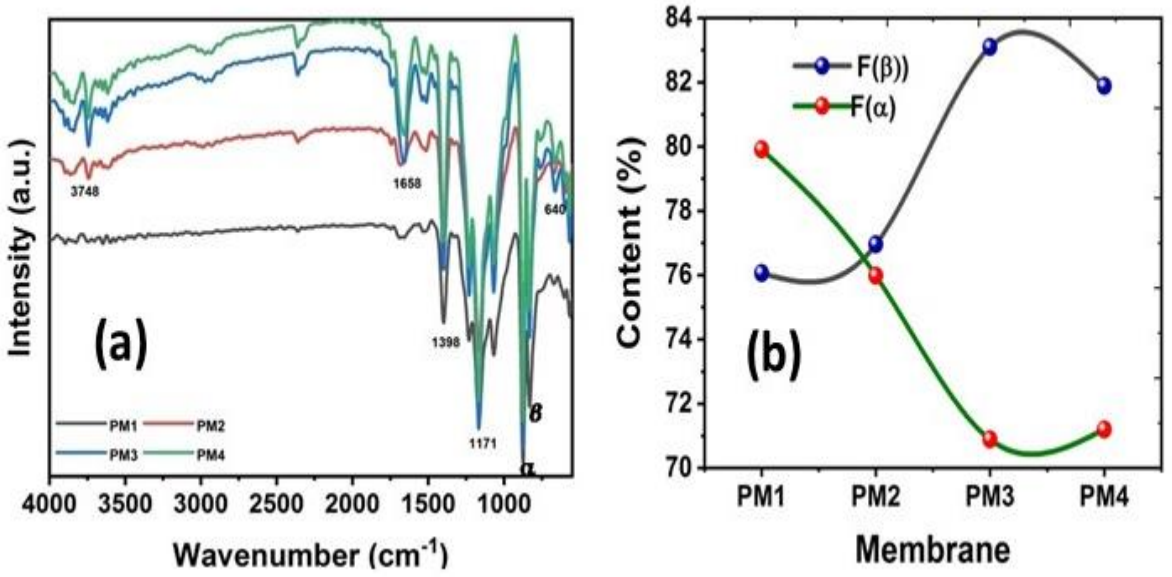

Figure 3.4: (a) FTIR spectra and (b) Fraction value of α and *β*-phases of pure PVDF and PVDF/TiO_2 composite membranes

3.3.1.d Diffusive Reflectance Spectroscopy: Optical Band Gap Analysis

Figure 3.5a shows the UV–Vis spectra of PVDF and PVDF/TiO_2 membranes. The figure depicts that absorption capability of the pure PVDF is minimal; as it did not absorb any light in the range 200 to 500 nm compared to TiO_2 incorporated membranes towards UV radiation which indicates an excellent optical response of PVDF/TiO_2 membranes to UV irradiation (Nor et al. 2016). This is attributed to the nanoparticle-polymer ionic interaction (Sharma et al., 2018). The corresponding band gap (difference of conduction and valence band energy and a significant parameter for a photo-catalytic reaction to happen) energy was calculated using Kubelka–Munk function (Escobedo et al. 2007) and the Tauc plot ($\alpha h\nu^2$ versus the energy for direct transition) was used to evaluate the band gap energy of the prepared composite membranes using Equation (3.13)

$$(\alpha h\nu)^n = A(h\nu - E_g) \quad (3.13)$$

where α, h, ν and E_g represent absorption coefficient, Planck constant (6.63×10^{-34} J s), speed of light (3×10^{8} m s^{-1}), and band gap energy, respectively, and n characterizes the nature of the transition process, i.e., n= 2 indicates the direct transition.

The calculated values of the band gap are 3.31, 3.52, and 3.59 eV for PM2, PM3, and PM4 membrane, respectively as shown in Figure 3.6b. It was observed that the value of band gap energy is higher than TiO_2 NPs (3.2 eV) due to the uniform distribution of NPs within the polymer matrix. These results suggest that the pure PVDF membranes act as support for the electron transport (Wang et al. 2017).

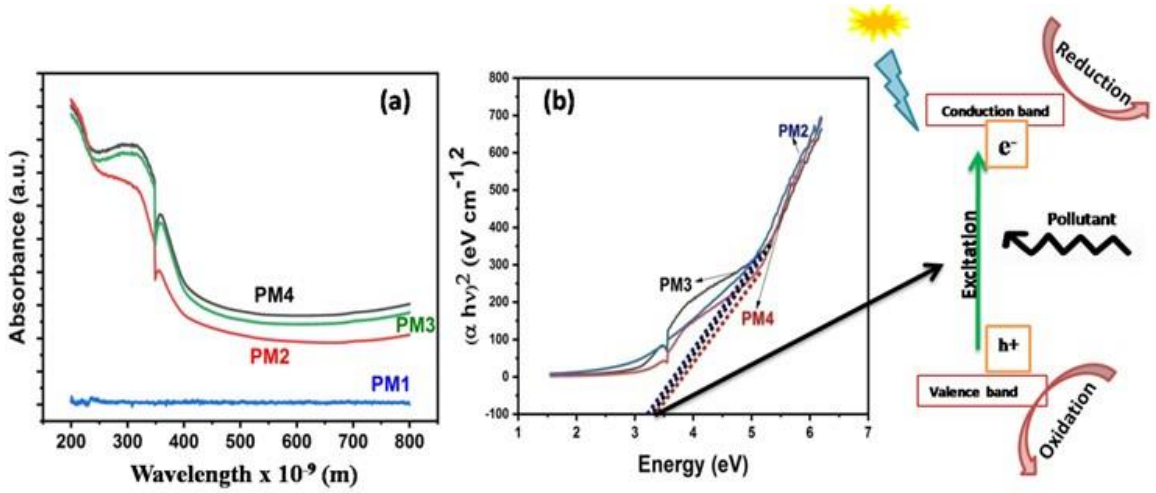

Figure 3.5: (a) DRS spectrum, (b) Band energy of PVDF/TiO_2 composite membranes

3.3.2 Phase Diagram

The quaternary phase diagrams obtained from the turbidimetric titration method for different concentrations of additives are shown in Figure 3.6. It is observed that on the introduction of TiO_2, the curve moves towards to the polymer/solvent axis, which means less amount of water is required for the precipitation or induce phase separation, thus the

thermodynamic stability of the solution reduces. The results are justified because of the presence of hydrophilic particle (TiO_2) having large affinity towards water creates more instability in the coagulation bath (Sadrzadeh and Bhattacharjee, 2013).

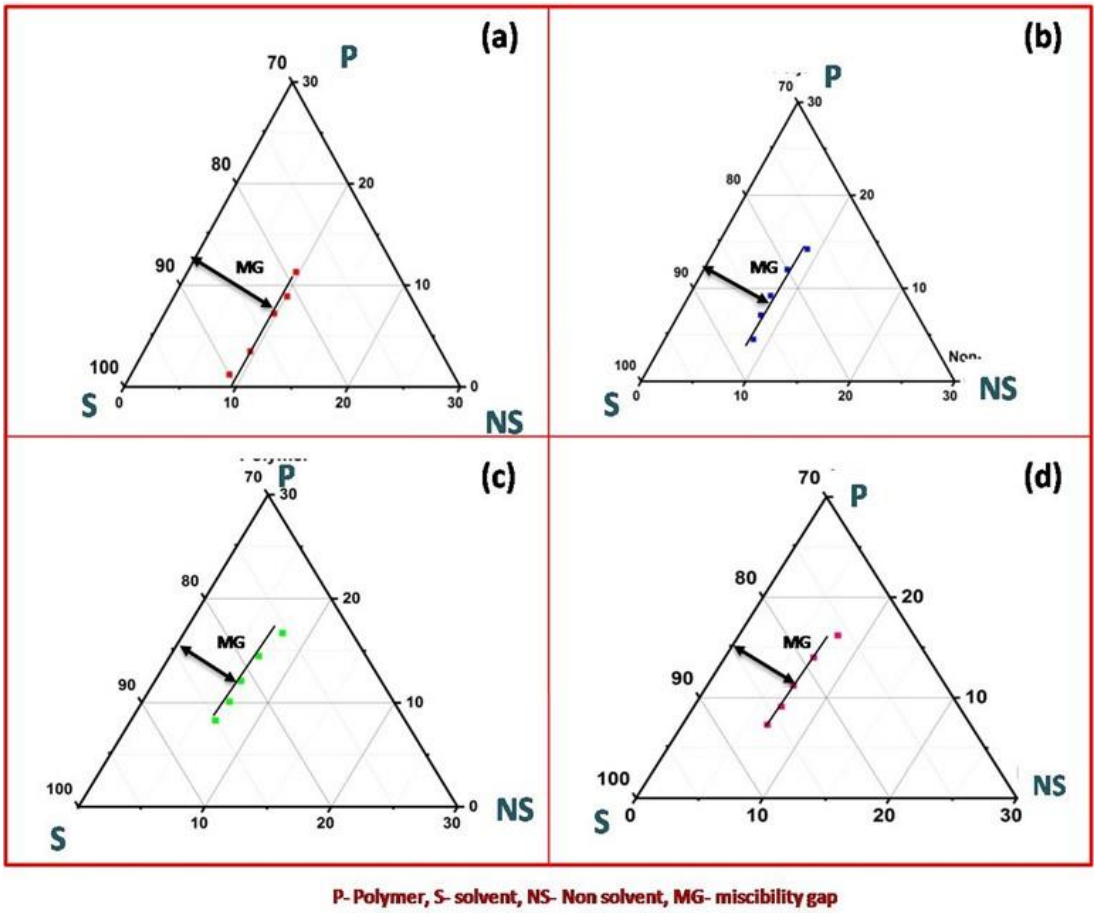

Figure 3.6: Ternary Phase diagram of PVDF/NMP (a) no TiO_2 (b) 1 wt% TiO_2 (c) 2 wt% TiO_2 (d) 3 wt% TiO_2

Figure 3.6 depicts that the addition of TiO_2 shifts the binodal line towards the polymer/ solvent axis, which leads to a decrease in the miscibility gap (MG). This induces greater instability and results in higher porosity (Gebru and Das 2017). The reduction in MG value increases the DSBC value. Membrane PM2 (1% TiO_2) has the lowest value of DSBC which implies that 1 wt% of TiO_2 has small effect on the thermodynamic

characteristic of casting solution due to low concentration while membrane PM4 (3wt% TiO_2) has the highest value of DSBC and confirms that the solution consisting of 3 wt% of TiO_2 is least stable. The DSBC determines the thermodynamic change of the polymeric casting solution. Since the amount of TiO_2 added is small, thermodynamic enhancement (thermodynamic change) is expressed in terms of the thermodynamic enhancement parameter (TE). The value of TE increases with increasing TiO_2 concentration, which signifies a higher value of thermodynamic enhancement in demixing due to the addition of the inorganic additive. The calculated value of MG, DSBC, and TE for different loadings of TiO_2 are listed in Table 3.2

Table3.2. Thermodynamic parameter for different membranes

Membrane	MG	DSBC (%)	TE
PM1	0.8	-	-
PM2	0.7	12.5	0.023
PM3	0.6	14.3	0.025
PM4	0.5	16.7	0.029

It was also observed that with increasing concentration of TiO_2, MG value decreases; this further leads to instant liquid-liquid de-mixing occurring in the coagulation bath, which promotes the formation of more voids within the membrane structure during immersion precipitation (Gebru and Das, 2017). Similar results are also reported in literature on the effect of additives (PEG, PVP) on MG (Gebru and Das, 2017).

The kinetics of phase inversion chaarcterizes the solvent/non-solvent demixing rate as it provides information about membrane structure. A kinetic parameter was determined using equations (3.4) to (3.8). The plot between relative concentration (C_t/ C_∞) of TiO_2 +

solvent (NMP) in a non-solvent (water) bath at different time intervals for different TiO_2 loadings is shown in Figure 3.7 a. This figure depicts that at the initial stage the diffusion rate is high and then it slows down as the polymer precipitates due to a decrease in the concentration gradient of organic solvent. This reduction will hinder the kinetics.

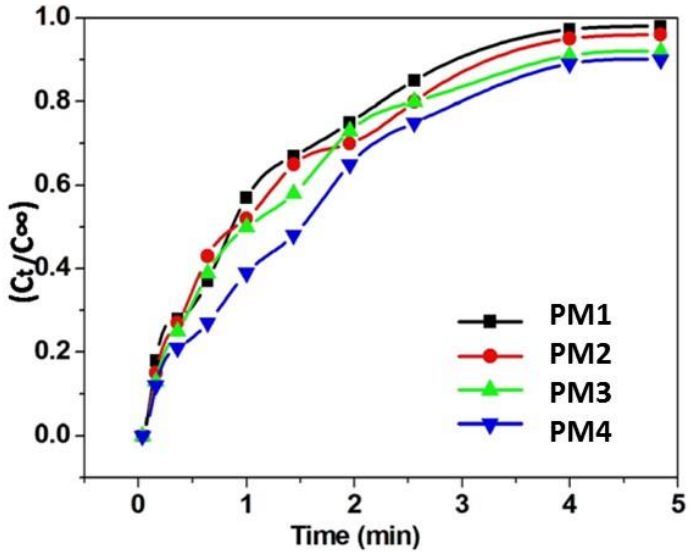

Figure 3.7: (a) Relative concentration versus time

The numerical value of slope (m) calculated from the graph between relative concentrations versus square root of time (Figure 3.7 b) and corresponding values of $\frac{D_{sa}}{\sqrt{D_{ns}}}$ are shown in Table 3.3

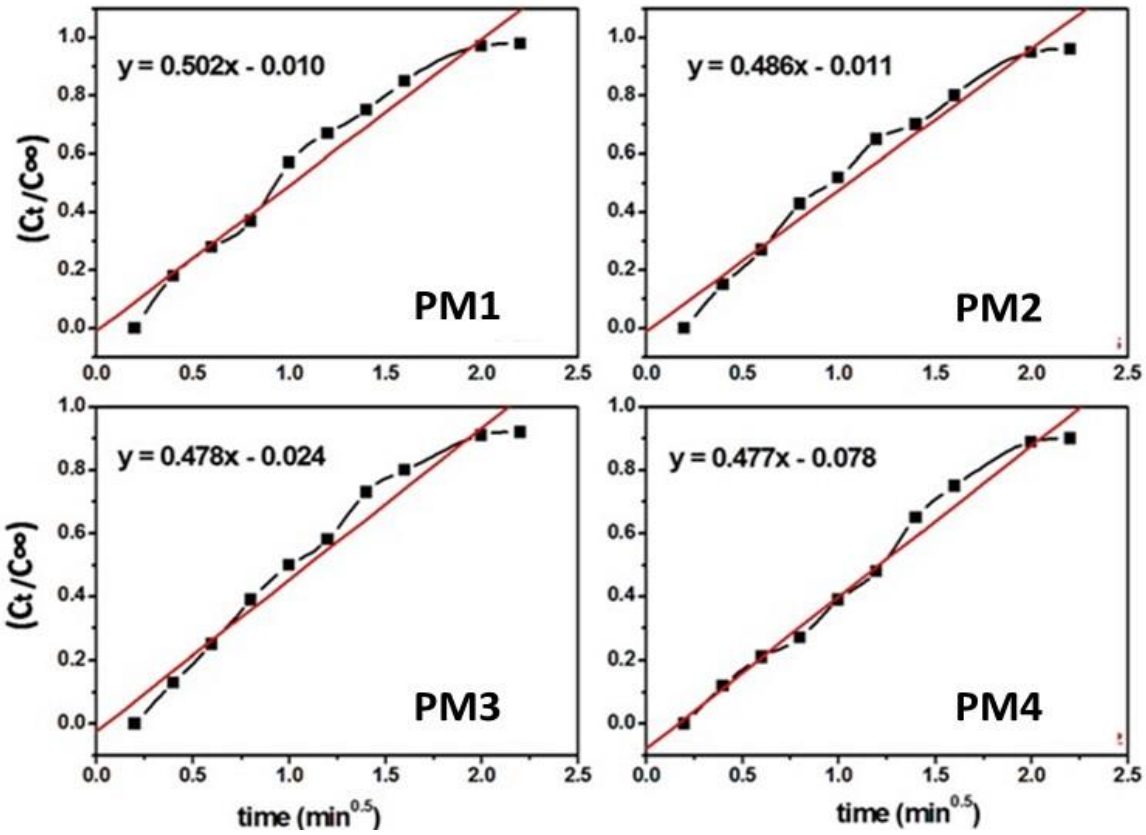

Figure 3.7 b) Relative concentration versus $t^{0.5}$ for different composite membranes

Table 3.3: Kinetic parameters of the polymeric solutions with different TiO_2 loading

Membrane	Intercept	M (min^{-12})	β	$T_o^{0.5}$	$\frac{D_{sa}}{\sqrt{D_{ns}}}$ (cm $min^{-1/2}$)	K
PM1	0.010	0.502	14.17166	0.01992	0.035423	0.064080
PM2	0.011	0.486	14.79167	0.02263	0.032856	0.020011
PM3	0.024	0.478	15.43478	0.05021	0.030969	0.017015
PM4	0.078	0.477	16.13636	0.16352	0.028321	0.042760

Results show that with increasing concentration of titanium oxide, the slope of the straight line decreases because of the increased viscosity due to addition of additives results in a slower rate of solvent diffusion, as a result mass transfer driving force decreases hence slope value declines. However, the small change in the value of the slope is observed due to the little difference in the loading of additives added. It should also be noticed that the interaction of the solvent with polymer affects the value of $\frac{D_{sa}}{\sqrt{D_{ns}}}$. TiO_2 being hydrophilic enhances the hydrophilicity of the membrane with an increase in its concentration. Increased hydrophilic property increases the water transfer rate thereby reduces the value of $\frac{D_{sa}}{\sqrt{D_{ns}}}$ as well as the kinetic parameter (Gebru and Das, 2017). The kinetic and thermodynamic parameters for different membranes are shown in Figure 3.7c. The figure depicts that by increasing the concentration of inorganic additive thermodynamic parameter increases, and the kinetic parameter decreases. With the addition of the TiO_2 the thermodynamic parameter increases and for the 2 wt% TiO_2 in PVDF casting solution this factor becomes more influential than the kinetic factor. This suggests that the synthesized membrane is expected to have high permeability, porosity, hydrophilic nature, and water flux compared to membranes PM and PM1. The results were expected because it is stated in the literature that the addition of the TiO_2 improves the performance of the membrane due to an increase in the flux (Mohsenpour et al., 2016). For PM4 membrane the increased viscosity makes kinetic factor more influential than thermodynamic factor thereby reducing permeability, porosity, hydrophilicity in comparison to PM3

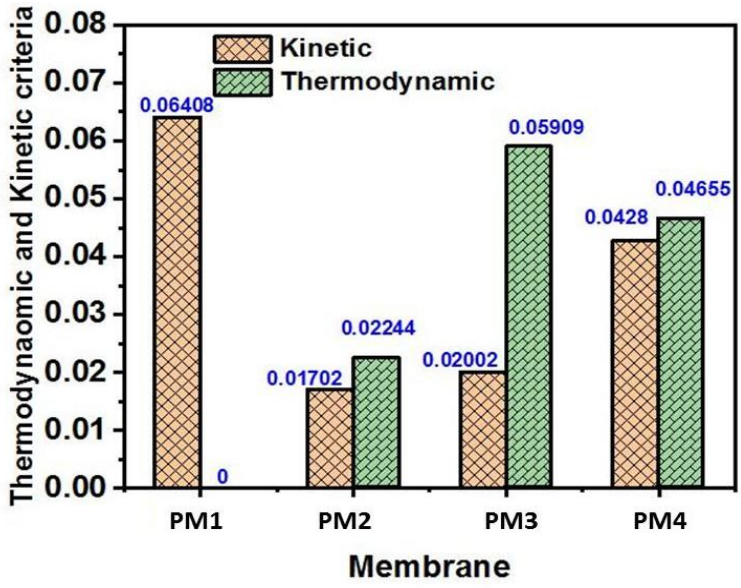

Figure 3.7: (c) Comparison of the thermodynamic & kinetic properties of the polymeric casting solution

3.3.3 High Resolution Scanning Electron Microscopy (HRSEM) Results

The membrane sample was characterized using a Field Emission Scanning Electron microscopy (HRSEM- Nova Nano SEM 450, FEI Company of USA (S.E.A.) PTE, LTD) to observe the effect of TiO_2 on the membrane morphology. Figure 3.8 depicts the cross-section image of the PVDF membrane. It was already concluded that with increasing concentration of TiO_2 in the polymer casting solution the thermodynamic parameter becomes larger than the kinetic parameter thus causing a faster exchange rate between the solvent and non-solvent because of greater tendency of miscibility with water due to the presence of hydrophilic material (Simone et al., 2018); as a result change in morphology from spongy to finger-like shape could be observed with increasing concentration as shown in Figure 3.8. However, at the highest concentration of TiO_2, the kinetic parameter becomes prominent, as shown in Figure 3.7c as a result, the demixing rate declines, finger-

like pores become more widened. Some sponge-like shapes could be observed because the increased viscosity creates a barrier for the solvent and non-solvent exchange, and also the blockage of pore occurs due to agglomeration of nano-particles at high concentration, thus decreasing the membrane permeability. In general, it can be said that the addition of the hydrophilic TiO_2 nano-particles into the casting solution generates the finger-like macro void, which would enhance the porosity and thus the permeability.

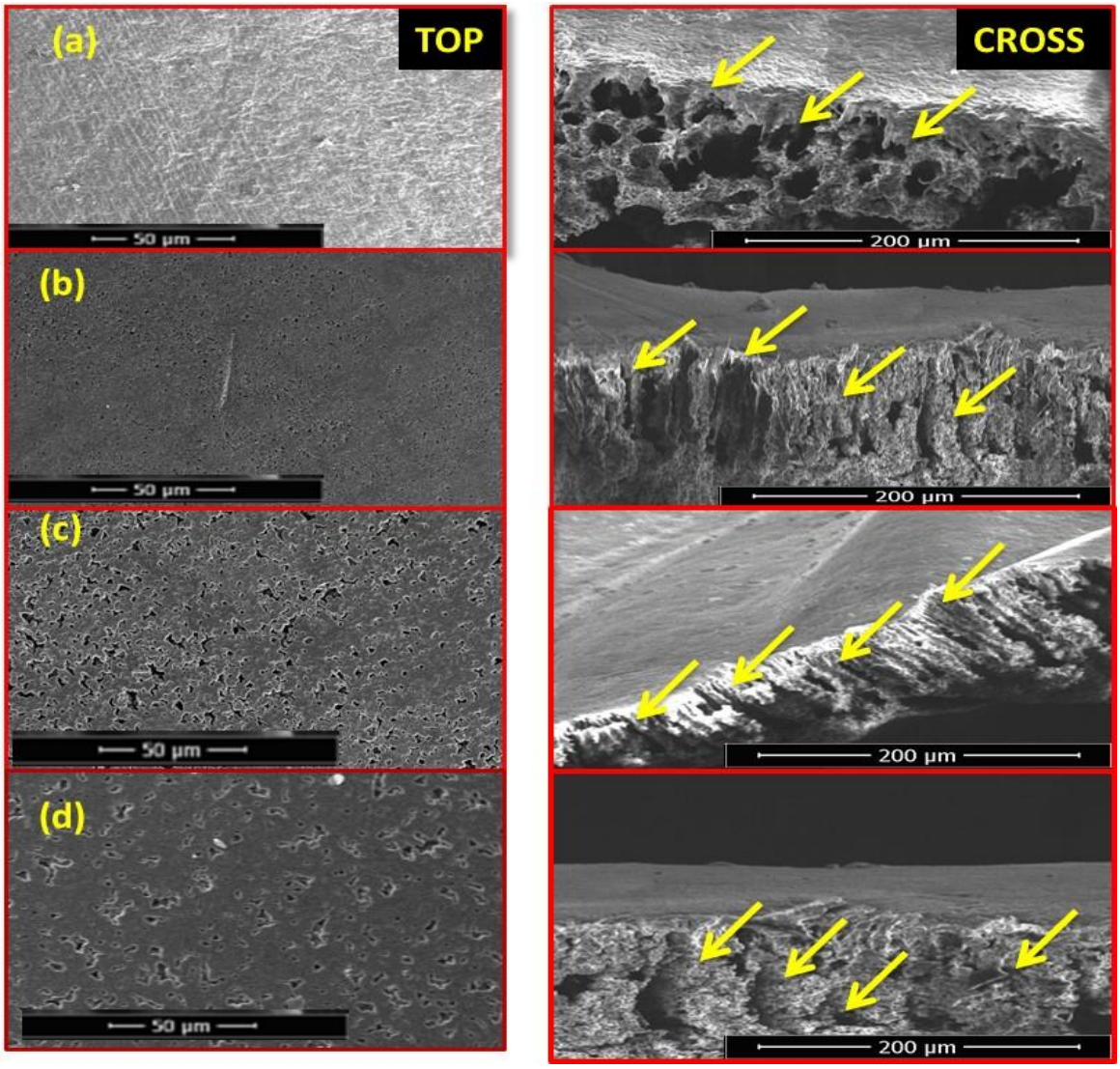

Figure 3.8: HRSEM images: (a) no TiO_2 , (b) 1 wt% TiO_2 , (c) 2 wt% TiO_2 , (d) 3 wt% TiO_2

Moreover, these figures also depict that the number of finger-like pores in the nano-composite membrane increases with an increase in TiO_2 loading. Thus it can be concluded that the addition of TiO_2 particles brings a drastic change in the morphology of membrane. It has been reported by Saljoughi et al. (2010) that at an excess concentration of TiO_2 nano-particle in polymer casting solution, the particles act as an anti-nucleating agent that suppresses the formation of macro voids due to excess of the multiple nuclei formation thus avoiding the existing nuclei to expand to from macro voids. Thus it becomes crucial that an adequate amount of nano-particles must be added to increases the chance of diffusion into the polymer phase, which increases the nuclei formation and ultimately leads to the finger-like macro voids.

3.3.4 Porosity, Pore size, tortuosity and Hydrophilicity of Membranes

The contact angle values determine the hydrophobicity of the membranes. Figure 3.9a depicts that the observed contact angle of PVDF/TiO_2 membranes is lower than the neat PVDF membrane. It is due to the high hydrophilic characteristic of TiO_2 NPs. It is observed that the contact angle value declines from 94.9 to 77.2° as the TiO_2 loadings increases from 0 to 3 wt% (Arif et al. 2019). These results suggest that the hydrophilicity of the PVDF/TiO_2 composite membrane is higher than PVDF membrane. A trend opposite to contact angle was observed for porosity and pore size (Figure 3.9b & 3.9c). The porosity increases from approx. 74 to 85 %, and the difference in porosity for PM1 and PM2 is more tangible compared to PM3 and PM4. It is due to increase in viscosity of the solution, which reduces the mass transfer rate between the solvent and the non-solvent, thus reducing the porosity and hence the pore size, with increasing inorganic TiO_2 concentration. The results are supported by the kinetic study result also. As already mentioned, that inverse

relationship exists between the tortuosity and porosity. Figure 3.9d shows decrease in tortuosity with increase in TiO_2 loadings.

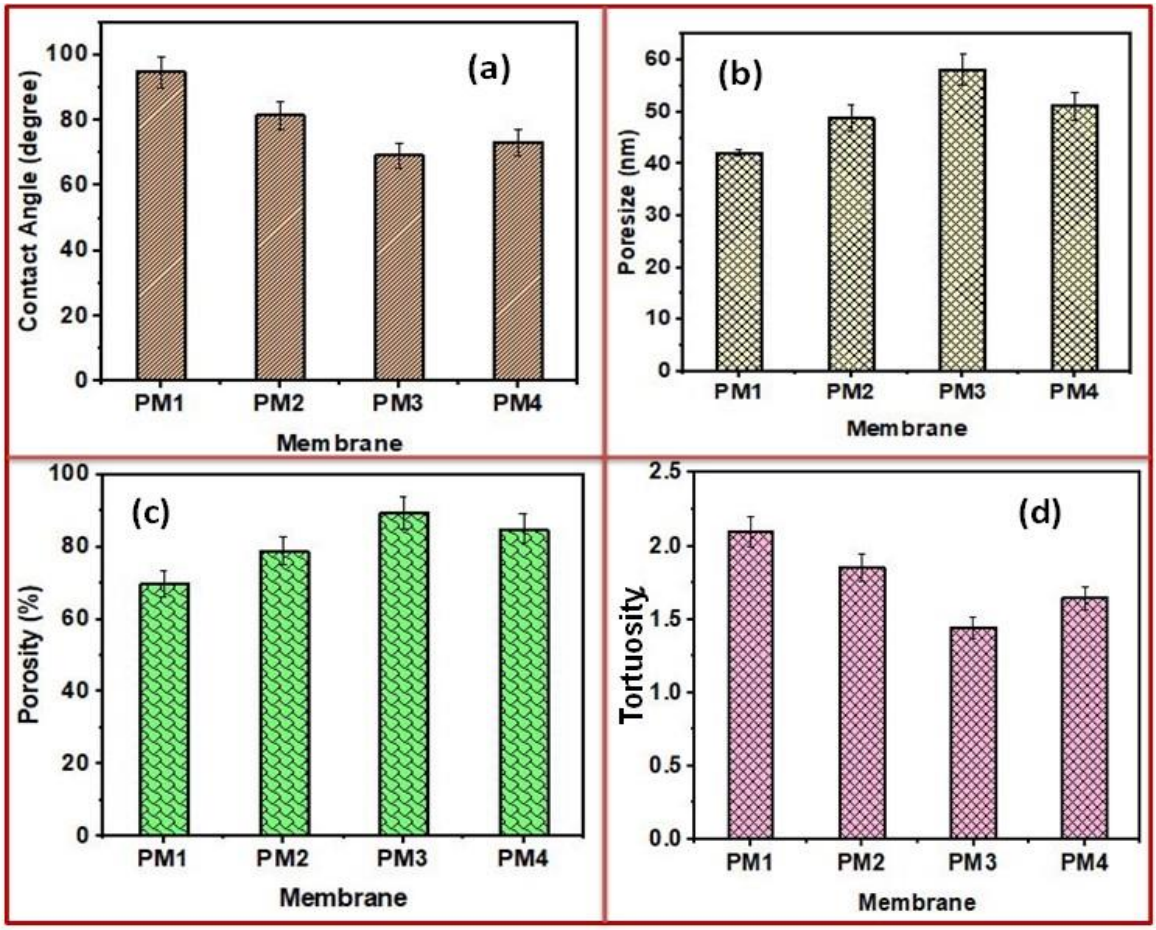

Figure 3.9: Change in (a) contact angle, (b) pore size, (c) porosity (d) tortuosity with TiO_2 loading

3.4 CONCLUSION

Anatase phase TiO_2 of crystallite size 15.89 nm was successfully synthesized using *Cajanus cajan* seeds extract. The influence of synthesized TiO_2 on membrane morphology was studied by investigating the thermodynamic and kinetic parameters. The following conclusion can be withdrawn for the particle and membrane synthesis:

- Nano-particles of TiO_2 of average size 20-30 nm using extract of *Cajanus cajan* were successfully synthesized.
- Pure and composite polymeric membranes of PVDF and PVDF/TiO_2, respectively were prepared via the phase inversion technique.
- FTIR spectroscopic and XRD analysis results indicated proper and uniform embedding of TiO_2 particles within polymer matrix. The DRS results confirmed that PVDF matrix acted as support for electron transport during photo-catalytic activity.
- PVDF/TiO_2 membrane exhibited lower contact angle compared to PVDF membrane. Composite membrane (PVDF/TiO_2) also had better hydrophilicity compared to PVDF membrane.
- The higher porosity and pore size of PVDF/TiO_2 membranes resulted in improved flux.
- Kinetic and thermodynamic parameters indicated improved phase separation resulting in higher porosity and water flux with increasing TiO_2 loading but at maximum loading (PM4 3 wt %) the rheological hinderance becomes more prominent due to increased viscosity hence delays the mixing rate and reduces the pore size formation, thus there exist a trade-off relation between thermodynamic and kinetic parameters.

3.5 REFERENCE

Arif Z, Sethy NK, Kumari L, Mishra, PK, Verma B (2019) Antifouling Behaviour of PVDF/TiO_2 Composite Membrane: A Quantitative and Qualitative Assessment Iranian Polymer Journal 28(2019)301–312.

Dai S, Wu Y, Sakai T, Du Z, Sakai H, Abe M Preparation of Highly Crystalline TiO_2 Nanostructures by Acid-assisted Hydrothermal Treatment of Hexagonal-structured NanocrystallineTitania/Cetyltrimethyammonium Bromide Nanoskeleton. Nanoscale Research Letter 5(2010) 1829–1835.

Damodar RA, Youa S, Chou H, Study the self-cleaning, antibacterial and photocatalytic properties of TiO_2 entrapped PVDF membranes. Journal of Hazardous Material 172 (2009) 1321-1328.

Gebru KA and Das C Impacts of solvents and additives on morphology, permeability and fouling performances, Chinese Journal of Chemical Engineering 25(2017) 911-923.

Jung JJ, Kim JF, Wang HH, Nicolo E, Drioli E, Lee YM (2016) Understanding the non-solvent induced phase separation (NIPS) effect during the fabrication of microporous PVDF membranes via thermally induced phase separation (TIPS). Journal of Membrane Science 514 (2016) 250-263

Jain A, Vaya A. Photocatalytic Activity of TiO_2 Nanomaterial. Journal of the Chilean Chemical Society 62 (2017) ISSN 0717-9707

Kurada KV and De S (2017) Role of Thermodynamic and Kinetic Interaction of Poly(Vinylidene Fluoride) With Various Solvents for Tuning Phase Inversion Membranes, Polymer Engineering and Science ,doi:10.1002/pen.24666

Lai CY, Groth A, Gray S, Duke M Preparation and characterization of poly(vinylidenefluoride)/nanoclay nanocomposite flat sheet membranes for abrasion resistance Water Research 57(2014)56 -66.

Li W, Liang R, Hu A, Huang Z, Zhau YN Generation of oxygen vacancies in visible light activated one-dimensional iodine TiO_2 photocatalysts RSC Advance 4(2014) 36959-36966.

Martins PM, Miranda R, Marques J, Tavares CJ, Botelho G, Lanceros-Mendez S, Damodar RA, Youa S Chou H, Comparative efficiency of TiO_2 nanoparticles in suspension vs. immobilization into PVDF–TrFE) porous membranes RSC Advance 6(2016) 12708-12716.

Mohsenpour S and Khosravanian A, Influence of additives on the morphology of PVDF membrane based on the diagram: thermodynamic and experimental study. Journal of Applied Polymer Scence 135(2018)46225-46235.

Mohsenpour S, Safekordi A, Tavakolmoghadam M, Rekabdar F, Hemmati M, Comparison of the membrane morphology based on the diagram using PVP as an organic additive and TiO_2 as an inorganic additive. Polymer, 97 (2016)559-568.

Moro P, Stampachiacchiere S, PiaDonzello M, Fierro G, Moretti G, A comparison of the photocatalytic activity between commercial and synthesized mesoporous and nanocrystalline titanium dioxide for 4-nitrophenol degradation: Effect of phase composition, particle size, and addition of carbon nanotubes**.** Applied Surface Science 359(2015)0293-305

Nor NAM, Jaafar J, Ismail AF, Mohamed MA, Rahman MA, Othman MHD, Lau WJ, YusofNPreparation and performance of PVDF-based nanocomposite membrane consisting of TiO_2 nanofibers for organic pollutant decomposition in wastewater under UV irradiation. Desalination 391(2016) 89–97.

Oh SJ, Kim N, Lee YT, Preparation and characterization of PVDF/TiO_2 organic–inorganic composite membranes for fouling resistance improvement. Journal of Membrane Science 345(2009)13-20.

Reuvers AJ, Altena FW, Smolders CA, Demixing and gelation behavior of ternary

cellulose acetate solutions. Journal of Polymer Science B Polymer Physics 24(1986)793-804.

Roshini R, Ardeshiri F, Peyravi M, Jahanshai MHighly permeable PVDF membrane with PS/ZnO nanocomposite incorporated for distillation process. RSC Advance 8(2018)23499-23515.

Sadrzadeh M and Bhattacharjee SJ, Rational design of phase inversion membranes by tailoring thermodynamics and kinetics of casting solution using polymer additives. Journal of Membrane Science 441(2013)31-44.

Saljoughi E, Amirilargani M, Mohammadi T, Effect of PEG additive and coagulation bath temperature on the morphology, permeability and thermal/chemical stability of asymmetric CA membranes. Desalination 262(2010)72-78.

Sharma M, Quamara JK, Gaur A Behaviour of multiphase PVDF in (1−x)PVDF/(x)$BaTiO_3$ nanocomposite films: structural, optical, dielectric and ferroelectric properties. Journal of Material Science: Material in Electronics 29(2018) 10875–10884

Shi N, Duan J, Su J, Huang F, Xue W, Zheng C, Qian Y, Chen S, Xie L, Huang W, Crystal polymorphism and enhanced dielectric performance of composite nanofibers of poly(vinylidene fluoride) with silver nanoparticles. Journal of Applied Polymer Science 128(2013) 1004–1010.

Shieh JJ and Chung TS, Effect of liquid-liquid demixing on the membrane morphology, gas permeation, thermal and mechanical properties of cellulose acetate hollow fibers. Journal of Membrane Science 140(1998)67-79.

Simone S, Figoli A, Criscuoli A, Carnevale M, Rosselli A, Drioli E, Preparation of hollow fibre membranes from PVDF/PVP blends and their application in VMD. Journal of Membrane Science 364(2010) 219-232.

Si Z, Zhang X, Liu, Y. et al. Revisiting the preparation of titanium dioxide: aerosol-assisted production of photocatalyst with higher catalytic activity than P25. Journal of Material Science 55 (2020) 565–576

Vinoth S, Kanimozhi G, Kumar H, Srinadhu ES, Satyanarayana N High conducting nanocomposite electrospun PVDF‐HFP/TiO_2 quasi‐solid electrolyte for dye‐sensitized solar cell. Journal of Material Science: Material in Electronic 30(2019) 1199–1213.

Wang C, Wu Y, Lu J, Zhao J, Cui J, Wu X, Yan Y, Huo P, Bioinspired Synthesis of Photocatalytic Nanocomposite Membranes Based on Synergy of Au-TiO_2 and Polydopamine for Degradation of Tetracycline under Visible Light. ACS Applied Material Interface 9(2017) 23687−23697.

Wang Q, Wang Z, Zhang J, Wang J, Wu Z Antifouling behaviours of PVDF/nano-TiO_2 composite membranes revealed by surface energetics and quartz crystal microbalance monitoring. RSC Advance 4(2014) 43590-43598.

Wei Y, Chu H, Dong B, Li X, Xia S, Qiang Z, Effect of TiO_2 nanowire addition on PVDF ultrafiltration membrane performance. Desalination 272(2011) 90–97

Wei YM, Xu ZL, Yang XT, Liu HL, Mathematical calculation of binodal curves of a polymer/solvent/nonsolvent system in the phase inversion process. Desalination 192(2006)91-104.

Yeow ML, Liu YT, Li K, Isothermal Phase Diagrams and Phase-Inversion Behavior of Poly(vinylidene fluoride)/Solvents/Additives/Water Systems. Journal of Applied Polymer Science 90 (2003) 2150-2155.